[11] Lighthill, M. J., "Dynamics of a dissociating gas, Part I—Equilibrium flow," J. Fluid Mech. **2**, 1–32 (1957).
[12] Lenard, M., Long, M. E., and Wan, K. S., "Chemical non-equilibrium effects in hypersonic pure air wakes," ARS Preprint 2675-62 (December 1962).
[13] Whalen, R. J., "Viscous and inviscid non-equilibrium gas flow," IAS Preprint 61-23 (January 1961).
[14] Mathews, D. L., "Interferometric measurement in the shock tube of the dissociation rate of oxygen," Phys. Fluids **2**, 170–178 (1959).
[15] Byron, S. B., "Interferometric measurement of the rate of dissociation of oxygen heated by strong shock waves," J. Chem. Phys. **30**, 1380–1392 (1959).
[16] Lin, S. C. and Teare, J. D., "Rate of ionization behind shock waves in air, II. Theoretical interpretation," Avco Research Rept. 115 (1962).
[17] Blackman, V., "Vibrational relaxation in oxygen and nitrogen," J. Fluid Mech. **1**, 61–85 (1956).
[18] Millikan, R. C. and White, D. R., "Vibrational energy exchange between N_2 and CO; The vibrational relaxation of nitrogen," J. Chem. Phys. **39**, 98–101 (1963).
[19] Nagamatsu, H. T., Geiger, R. E., and Sheer, R. E., Jr., "Real gas effects in flow over blunt bodies at hypersonic speeds," J. Aerospace Sci. **27**, 241–251 (1960).
[20] Nagamatsu, H. T., Geiger, R. E., and Sheer, R. E., Jr., "Hypersonic shock tunnel," J. ARS **29**, 332–340 (1959).
[21] Nagamatsu, H. T., Sheer, R. E., Jr., Osburg, L. A., and Cary, K. H., "Design features of the General Electric Research Laboratory hypersonic shock tunnel," General Electric Research Lab. Rept. 61-RL-2711C (1961).
[22] Humphrey, R. L., Little, W. J., and Seeley, L. A., "Mollier diagram for nitrogen," Arnold Engineering Development Center AEDC-TN-60-83 (1960).
[23] Alpher, R. A. and Greyber, H. D., "Calculation of shock hugoniots and related quantities for nitrogen and oxygen," Phys. Fluids **2**, 160–161 (1958).
[24] Smith, C. E., Jr., "Thermodynamic properties of nitrogen," Lockheed Missiles and Space Co., Rept. 6-90-62-111 (1962).
[25] Hilsenrath, J. and Beckett, C. W., "Tables of thermodynamic properties of argon-free air to 15,000°K," Arnold Engineering Development Center TN-56-12 (1956).
[26] Hurle, I. R., Russo, A. L., and Hall, J. G., "Experimental studies of vibrational and dissociative nonequilibrium in expanded gas flows," AIAA Preprint 63-439 (1963).

AUGUST 1965 AIAA JOURNAL VOL. 3, NO. 8

Hypersonic Viscous Effects on Free-Flight Slender Cones

BAIN DAYMAN JR.*

Jet Propulsion Laboratory, California Institute of Technology, Pasadena, Calif.

An experimental study was performed in order to determine the effects of various parameters upon cone aerodynamics in the hypersonic regime at Reynolds numbers as low as 7800/in. The use of free-flight models eliminated the need for evaluating sting interference and made practical accurate measurement of drag forces down to 8×10^{-4} lb and pitching moments as low as 2×10^{-4} in-lb. The effects of model to total temperature ratios of 0.45 (gun launch) and 0.87 (wire release) for 6° through 15° half-angle cones on total drag and static stability were investigated at Mach numbers from 6 to 10 for values of the viscous Knudsen number up to $M_\infty/(R_{D_\infty})^{1/2} = 0.28$. Limited nose-blunting effects were also investigated. Conical shock viscous drag theory agrees quite favorably with the experimental data. Use is made of trends predicted by theory in order to compare the data of this paper with available hypersonic viscous cone drag data.

Nomenclature

A = model base area
C_f = flat-plate local skin-friction coefficient
C_{DT} = total effective drag coefficient of oscillating model = drag/$q_\infty A$ (no correction for base pressure)
$C_{D_{0_T}}$ = total drag coefficient at zero angle of attack = $C_{D_T} - \epsilon\alpha_{\text{env}}^2$, deg^2
ΔC_{D_v} = viscous interaction drag = $C_{D_{0_T}} - [C_{D_{0_T}}]$ at $\bar{V}_\infty{}' = 0$
C_{m_α} = effective pitching moment slope/rad = moment/$q_\infty AD$
C_{N_α} = normal force coefficient slope/rad = (normal force)/$q_\infty A$
C_c = cone-surface form of Chapman-Rubesin viscosity coefficient = $\mu_w T_c/\mu_c T_w$
C_∞ = freestream form of Chapman-Rubesin viscosity coefficient = $\mu_w T_\infty/\mu_\infty T_w$
D = model base diameter
K = hypersonic viscous parameter (based on model length) = $M_\infty/(R_{L_\infty})^{1/2}$
K' = hypersonic viscous parameter (based on model base diameter) = $M_\infty/(R_{D_\infty})^{1/2}$
L = model length (for blunted models, length taken as that for sharp-nose model of same diameter)
M = Mach number
P = pressure
P_0' = freestream pitot pressure
q = dynamic pressure
r = radius
$Re/\text{in.}$ = Reynolds number/in.
R_D = Reynolds number based on model base diameter
R_L = Reynolds number based on model length, L
R_x = Reynolds number based on distance from flat-plate leading edge
t = time
T = temperature
$\bar{V}$ = hypersonic viscous parameter = $M(C/R_L)^{1/2}$
$\bar{V}'$ = hypersonic viscous parameter = $M(C/R_D)^{1/2}$
V_m = model velocity relative to ground
$X_{c.g.}$ = distance of c.g. aft from model nose (sharp)
$\bar{\chi}_L$ = hypersonic viscous interaction parameter = $M_c^3(C_c/R_{Lc})^{1/2}$
α = angle of attack
α_{env} = envelope of oscillation
β = slope of drag curve (based on model length) = $dC_{D_{0_T}}/dK$
β' = slope of drag curve (based on model base diameter) = $dC_{D_{0_T}}/dK'$

Presented as Preprint 64-46 at the AIAA Aerospace Sciences Meeting, New York, N.Y., January 20–22, 1964; revision received April 14, 1965. This paper presents the results of one phase of research carried out at the Jet Propulsion Laboratory, California Institute of Technology, under Contract No. NAS 7-100, sponsored by NASA.

* Manager, Aerodynamic Facilities Section. Associate Fellow Member AIAA.

$\beta_{\bar{v}}$ = slope of drag curve (based on model length) = $dC_{D0T}/d\bar{V}$
$\beta_{\bar{\chi}}$ = slope of drag curve (based on model length) = $dC_{D0T}/d\bar{\chi}$
$\tilde{\beta}_{\bar{v}\infty}'$ = $\beta_{\bar{v}\infty}'$ normalized to $\sigma = 10°$ and $T_w/T_0 = 0.5$
ϵ = slope of drag curve = $dC_{DT}/d\alpha_{env}^2$, deg^2
Γ = $\beta_{\bar{v}\infty}'$
σ = cone semiapex angle
μ = viscosity

Subscripts

B = model base
c = cone surface (at outer edge of boundary layer)
N = model nose
0 = nominal freestream total
w = model wall
∞ = nominal freestream

Introduction

BECAUSE of their basic simplicity, cones were a natural beginning for both theoretical and experimental studies of three-dimensional viscous aerodynamics. Various authors[1–6] have made significant contributions by the formulation of a theoretical understanding (Ref. 7 contains an excellent bibliography of additional work in this field). During the past several years, experimenters[8–15] have published limited data on such cones, but because of the lack of systematic variation of parameters other than the Reynolds number, it is difficult, if not impossible, to obtain an understanding of the effects of any one parameter. In order to provide information for evaluating the effects of various parameters such as cone angle, nose bluntness, and wall temperature along with Mach and Reynolds numbers, a program was initiated in the hypersonic wind tunnel at the Jet Propulsion Laboratory (JPL). The negligible real gas effects simplify the use of these data for the further development of a theoretical model.

All in all, the measurement of drag and stability of slender cones at very low Reynolds numbers can be a challenging problem. Not only is it extremely difficult to construct and use a balance sensitive enough to accurately measure loads on the order of 10^{-3} lb and less, but the interference of a sting or any other support could substantially affect the measurements relative to the interference-free condition. Rather than take on a time-consuming balance-development task and yet be faced with assessing the magnitude of support interference, it was decided to use the free-flight technique[16] in a conventional wind tunnel to obtain data on small, slender cones in hypersonic flow at low Reynolds numbers.

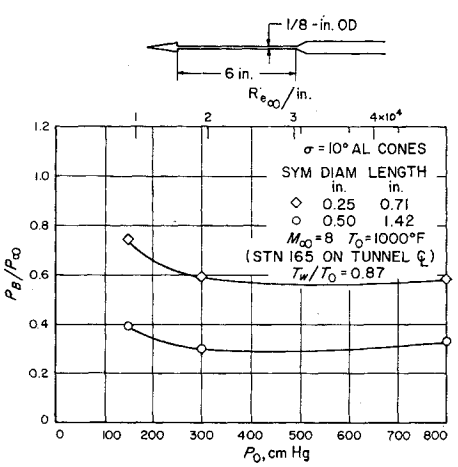

Fig. 1 Model base pressure.

Interference Effects

Either side or sting supports are likely to cause a large change in the base pressure relative to the noninterference case. A description of the effects of transverse supports on the wake shape for both spheres and cones is given in Ref. 17. Wires less than 1% of the model base diameter can substantially distort the wake shape. This is indicative that the base pressure has been altered.

The effect of sting interference on base pressure is well known. An example of this interference was obtained during this study and appears in Fig. 1. An increase in the ratio of sting to model base diameter from 0.25 to 0.50 doubles the base pressure (from P_B/P_∞ = 0.3–0.6). As the boundary-layer thickness on these cones can be on the order of the model radius, a pressure disturbance on the base can, in principle, feed forward through the subsonic portion of the thick boundary layer and consequently distort the boundary layer on the cone surface. The magnitude of the resulting effect on the drag and stability data is not known. However, such an effect should not be ignored; it must be investigated.

A similar situation exists in the use of low-density wind tunnels where the boundary-layer thickness may be about half of the nozzle radius. Any variation in the test chamber (plenum) pressure affects the nozzle exit Mach number. The only way that this could occur would be for the pressure variation to feed upstream into the nozzle through the boundary layer and change the characteristics of the boundary layer. This change in Mach number is shown in Fig. 2 (data from Ref. 18).

Test Procedure

The small thin-shell models were made out of magnesium, aluminum, or brass. The material density was chosen to limit the model flight accelerations to the region of 6 to 20 g's. The models were released into free-flight trajectories across the viewing window of the 21-in. hypersonic wind tunnel by two methods. The equilibrium wall-temperature models were supported on a vertical wire at the window upstream edge and were released into flight by rupturing the 0.012-in. D wire at a notch located within the model.

The cold wall-temperature models were launched against the airstream by a pneumatic tube located downstream of the window. The launch tube was far enough downstream (6 in.) so that no wake interference was propagated upstream to the model base when the model was in view. The cone models were mounted on a piston sabot, initially contained within the launch tube, which was accelerated to 20–30 fps in a distance of 1 ft by air at about $\frac{1}{2}$ atm pressure.

The free-flight trajectories were recorded on 35-mm movie film at about 4000 frames/sec. The drag is obtained by measuring the model position as a function of time and then determining the model acceleration. One of the several procedures used to obtain acceleration assumes negligible variation of acceleration during the trajectory. When the magnitude of model acceleration is large enough to cause a substantial variation in the acceleration during the visible trajec-

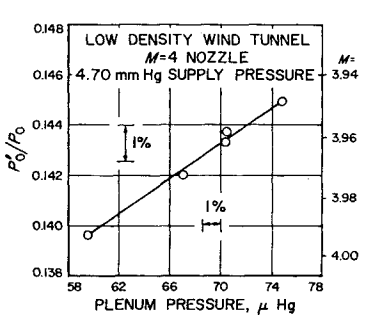

Fig. 2 Effect of plenum pressure on Mach number.

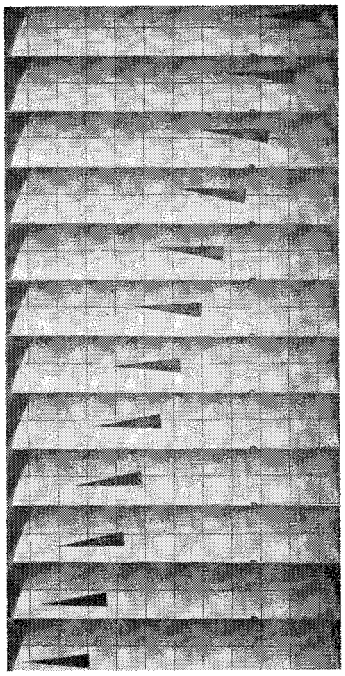

Fig. 3 High-speed movie sequence of gun-launch model during one cycle of oscillation.

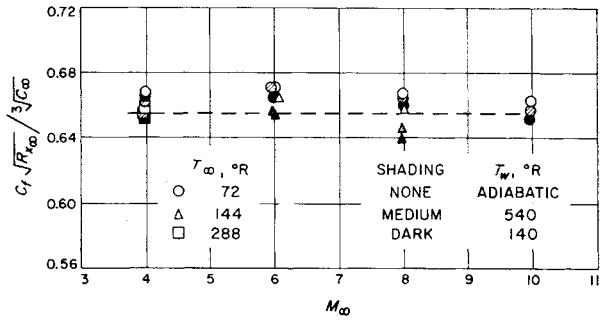

Fig. 4 Theoretical flat-plate laminar boundary-layer local skin friction.

tory, a more sophisticated method of data reduction[19,20] is required. The pitching moment is directly related to the oscillation frequency. A sample cycle of oscillation from the film is in Fig. 3. The weights and dimensions of all models were accurately measured. However, sufficiently accurate determination of center-of-gravity position and moment of inertia was limited to the 0.50-in. D cone models. A more complete description of the test procedures (models, launching techniques, data reduction, etc.) is included in Ref. 21.

Supporting Studies

Experimental

In order to obtain reliable drag and stability data, the test-section flow conditions and the model wall temperatures must be known. Careful vertical flow calibrations at the upstream end of the viewing window were made after each model was launched. At the end of the test, similar pitot pressure profiles were made at the downstream end of the window. The flow had less than 1% variation in dynamic pressure within the flight region (see Ref. 22). The requirement of good flow for observing viscous effects by the use of the free-flight technique is due to the fairly large region through which the model travels. Additional flow calibrations for both the $M = 6$ and $M = 8$ nozzles were obtained several times after the test with a precisely calibrated and leak-tight pressure system. Therefore, the dynamic pressure and other pertinent flow parameters are known to within 1% for the $M = 6$ and $M = 8$ data. Since this was not done for the $M = 10$ nozzle, the $M = 10$ data are subject to question (about ±6% rather than ±2% as for the other data).

A thermocouple was installed in both a wire-supported model and a sabot-launched model. Actual temperature measurements and tunnel flow calibrations appear in Ref. 21.

Theoretical

In order to develop a feeling for the effect of various parameters upon the hypersonic viscous drag of cones, theoretical studies were performed which included the range of conditions studied in this experimental paper. The conical shock theory of Ref. 2 is used rather than the normal shock theory. This is justified, since most of the flow in the boundary layer (which can be about the cone radius in thickness) goes through the conical portion of the shock. Convenient equations for this theory are presented in Ref. 13. The equations were programed on a computer in order to obtain a significant number of systematic comparisons. The only change made from Ref. 13 is the form of the similar friction drag. Machine-computed laminar boundary-layer skin-friction coefficients[23] become independent of Mach and Reynolds numbers as well as wall-temperature ratios when presented (Fig. 4) in the form of $C_f(R_{x_\infty})^{1/2}/(C_\infty)^{1/3}$ (which yields less than 5% spread in data for the experimental conditions of this paper) rather than the usual form of $C_f(R_{x_\infty}/C_\infty)^{1/2}$ (which gives a 12% spread in data). For skin-friction calculations, the value of $C_f(R_{x_\infty})^{1/2}/(C_\infty)^{1/3} = 0.655$ was used.

Figure 5 presents theoretical values of ΔC_{D_v} as a function of $\bar{V}_\infty$ (based upon model length) with cone angle as the variable. The effect of cone angle is quite large. This large effect still exists when either $\bar{V}_c$ or $\bar{\chi}_L$ is used. When the viscous parameter $\bar{V}_\infty'$ (based upon model diameter) is used, the theoretical effect of cone angle on ΔC_{D_v} is appreciably reduced and becomes small (Fig. 6) for values of $\bar{V}_\infty' < 0.1$. Similar comparisons result for the entire Mach number range studied of $4 < M_\infty < 20$. Mach number effect on ΔC_{D_v} is minimized when the viscous parameter $\bar{V}_\infty'$ or $\bar{V}_\infty$ is used (Fig. 7). The use of either $\bar{V}_c$ or $\bar{\chi}_L$ causes a large effect of Mach number on the viscous drag. Similar comparisons result during the entire cone angle range studied of $6° < \sigma < 15°$. Effect of wall temperature to total temperature ratio on the cone viscous drag is shown in Fig. 8. The magnitude of the effect is a function of the viscous parameter; as the parameter increases, the effect on viscous drag of wall-temperature ratio increases. In this figure, the values used for the viscous parameters are $\bar{V}_\infty' = 0.11$ and $\bar{\chi}_L = 1.6$. The

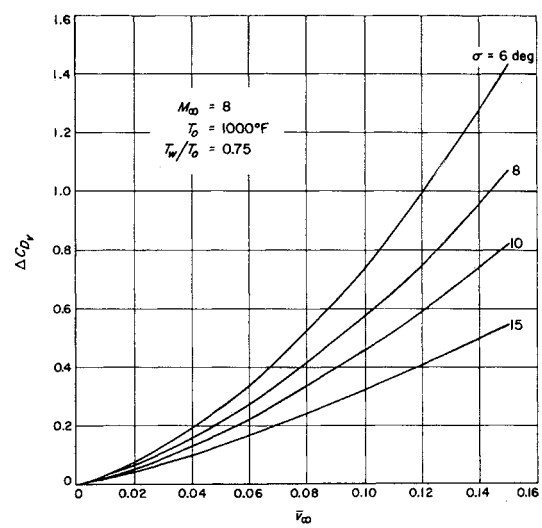

Fig. 5 Effect of cone angle on viscous drag (ΔC_{D_V} vs $\bar{V}_\infty$), theory.

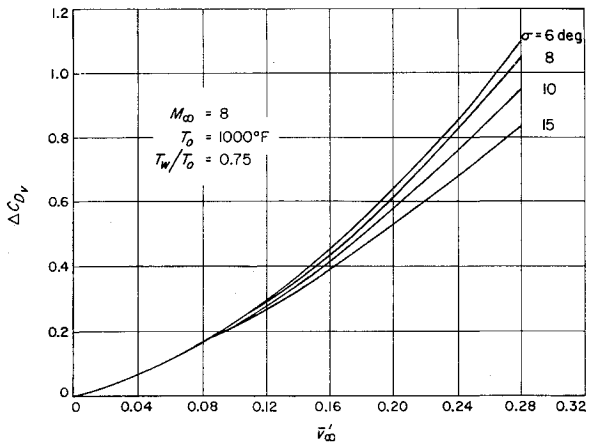

Fig. 6 Effect of cone angle on viscous drag (ΔC_{D_V} vs V_∞'), theory.

reason for these choices will be discussed later. The effect shown at $M_\infty = 8$ is increased with increasing Mach number. If the viscous parameter is in the form of $M_\infty/(C_\infty R_{D_\infty})^{1/2}$, the effect of wall-temperature ratio is significantly reduced, becoming less than 20% for the conditions studied ($8 < M_\infty < 15$, $6° < \sigma < 15°$) when presented in the manner of Fig. 8.

The relationships between $\bar{V}_c$ and $\bar{\chi}_L$ with $\bar{V}_\infty$ are based upon results in Ref. 24.

Experimental Results

The data of this paper were originally presented in Ref. 21. At that time preliminary means were used to reduce the data. Since then, the data have been rereduced in an exact manner, and the $M = 6$ and $M = 8$ nozzles have been check-calibrated several times. All questionable $M = 6$ and $M = 8$ data have been eliminated. However, even though not as precise as the $M = 6$ and $M = 8$ data, some $M = 10$ data of Ref. 21 are included in this paper in order to aid in establishing a Mach number effect. Real gas effects, though small, are included in the data reduction.

Parameters Investigated

The following parameters were investigated during this study: 1) Mach number (6, 8, 10), 2) unit Reynolds number (0.8×10^4 to 25×10^4/in.), 3) model size (0.10, 0.25, 0.50, 1.00, 1.50-in. D), 4) cone angle ($\sigma = 6°, 8°, 9°, 10°, 15°$), 5) nose bluntness ($r_N/r_B = 0, 0.05, 0.20$), 6) model wall-temperature to total-temperature ratio (0.45 and 0.87), 7) oscillation envelope (0° to 18°), and 8) center-of-gravity location (0.45 to 0.69 model length from nose).

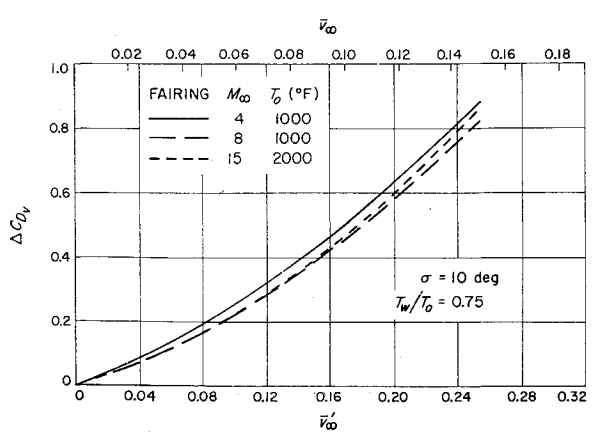

Fig. 7 Effect of Mach number on cone viscous drag, theory.

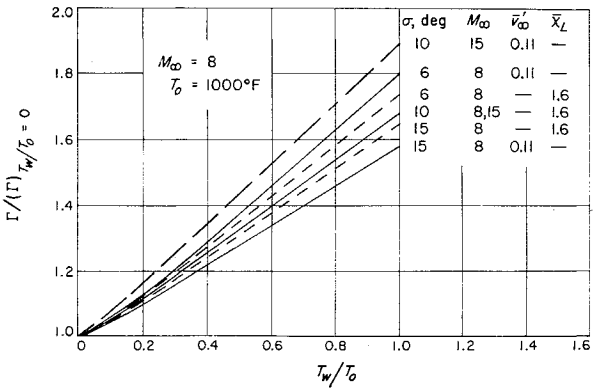

Fig. 8 Effect of wall-temperature ratio on cone viscous drag, theory.

Drag

Oscillation envelope effects

The presented drag coefficients do not have any corrections for base pressure. For the nonviscous cases, it is assumed (Fig. 1) that the cone base pressure is one-fourth of the free-stream static pressure. These theoretical data are indicated by an "X" on the drag plots. Since the models were generally launched at small angles of attack in order to obtain static stability data, the measured average total drag was decreased by an estimated drag increment in order to obtain drag at zero angle of attack. This relationship of drag as a function of oscillation envelope for a 10° cone at $M_\infty = 8$ is shown in Fig. 9. Theoretically, and for the considerably less viscous (higher Reynolds number) experimental case, this plotted relationship is linear. It appears that the viscous case also yields a linear relationship. This also has been borne out by the work in Ref. 14.

To correct the drag to zero angle of attack, the constants shown in Table 1 (based on Newtonian calculations corrected to experimental data) were used in the expression $C_{D_0T} = C_{D_T} - \epsilon\alpha_{\text{env}}^2$ (deg^2). Since the drag correction increments in Table 2 are small (usually less than 0.02), there is negligible loss in accuracy in going from C_{D_T} to C_{D_0T}.

In addition, the effects of the model base cavity and the holes necessary for wire launch were determined. Because of this rather extensive list of parameters, it was not possible to define conclusively the effects of every parameter. Variables, test conditions, and reduced data are listed in Table 2.

Method of data presentation

Viscous drag data have been presented as a function of several definitions of the hypersonic viscous parameter. Two of the more common forms of the viscous parameter are $\bar{V}_\infty$[13,15] and $\bar{\chi}_L$.[14] Each has its own particular

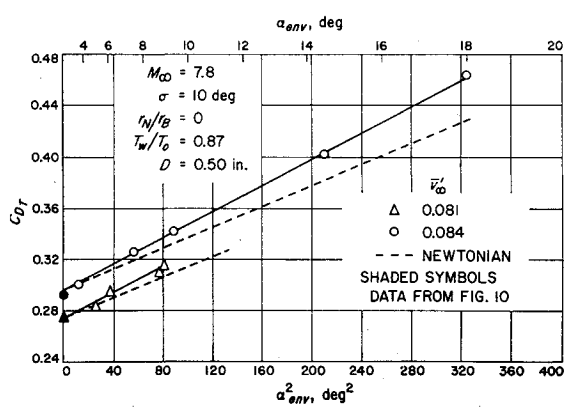

Fig. 9 Effect of oscillation envelope on total drag.

Table 1 Constants used to correct drag to zero angle of attack

σ, deg	$\epsilon \times 10^4$
6	5.5
8	5.2
9	5.1
10	5.0
15	4.4

reason for being used: $\bar{V}_\infty$ [i.e., $M_\infty(C_\infty/R_{L_\infty})^{1/2}$] yields similar friction drag that is essentially independent of Mach number, and $\bar{\chi}_L$ [i.e., $M_c^3(C_c/R_{L_c})^{1/2}$] is the basic parameter in the theoretical equations of viscous drag.[2] The relatively simple parameter K [i.e., $M_\infty/(R_{L_\infty})^{1/2}$] was used in Ref. 21. Each of these three forms is adequate when the variable is model Reynolds number. However, none is capable of sensibly comparing viscous data for a variety of cone angles and Mach numbers. As was shown,[21] the use of K' [i.e., $M_\infty/(R_{D_\infty})^{1/2}$] minimized the effect of cone angle on viscous drag. So a combination parameter $\bar{V}_\infty'$ [i.e., $M_\infty(C_\infty/R_{D_\infty})^{1/2}$] was chosen as the viscous parameter in this paper in order to minimize cone angle and Mach number effects. The only variable that it does not normalize out is the effect of wall-temperature ratio. The parameter $M_\infty/(C_\infty R_{D_\infty})^{1/2}$ will minimize (both experimentally and theoretically) the effects of wall-temperature ratio variations on the viscous cone drag as well as both cone angle and Mach number (Table 3).

Base conditions

The base condition was quite thoroughly documented. It consists of the sharp-nose, 10° half-angle, adiabatic-wall cone at $M_\infty = 8$ for small envelopes of oscillation ($\sigma_{env} < 5°$). The complete Reynolds number and model size ranges for this case were investigated. The results are shown in Fig. 10. The data spread in the vicinity of $\bar{V}_\infty' = 0.083$ is a direct indication of the data scatter to be expected for the means

Table 2 Tabulation of JPL test conditions and final data; a) $\sigma = 6°, 8°, 9°, 15°$; b) $\sigma = 10°$

a)

Test	Run	M_∞	P_o (cm Hg)	T_o (°F)	T_w/T_o	σ (deg)	D (in.)	r_N/r_B	$R_{L_\infty} \times 10^{-4}$	$M_\infty/\sqrt{R_{L_\infty}}$	$\bar{V}_\infty'$	$\bar{V}_\infty$	$\bar{V}_c$	$\bar{\chi}_L$	σ_{env} (deg)	C_{D_T}	$C_{D_{o_T}}$	X_{cg}/L	$-C_{m_\sigma}$/rad
21-150	78.1	7.88	449	1005	0.87	6	0.10	.0	1.34	0.068	0.122	0.056	0.042	1.98	1.0	0.358	0.356		
↓	98 1	7.78	120	1005	0.87	6	0.50	0	1.81	0.058	0.105	0.048	0.036	1.66	3.5	0.307	0.300		
	79 1	7.84	301	1005	0.87	6	0.50	0	4.49	0.037	0.068	0.031	0.023	1.08	5.5	0.221	0.204	0.458	2.45
	99.2	7.79	150	1005	0.43	6	0.50	0	2.25	0.052	0.105	0.048	0.036	1.65	8.0	0.297	0.262	0.455	2.49
	79.2	7.84	300	1000	0.45	6	0.50	0	4.42	0.037	0.074	0.034	0.026	1.21	0.5	0.197	0.197		
	63.2	7.84	300	1000	0.45	6	0.50	0	4.42	0.037	0.074	0.034	0.026	1.20	1.5	0.201	0.200		
	75.2	7.88	449	1000	0.47	6	0.50	0	6.56	0.031	0.061	0.028	0.022	1.00	0.3	0.177	0.166		
	81.2	7.84	301	1010	0.45	6	0.50	0.05	4.42	0.037	0.074	0.034	0.026	1.21	1.4	0.184	0.183	0.458	2.21
↓	68.2	7 80	183	1005	0.42	6	0.50	0.20	2.77	0.047	0.094	0.043	0.033	1.51	0.4	0.239	0.239		
21-150	93.1	7.78	120	1000	0.87	8	0.10	0	0.28	0.148	0.230	0.122	0.082	3.46	4.4	0.643	0.633		
↓	92 1	7.78	120	1000	0.87	8	0.10	0	0.28	0.148	0.230	0.122	0.082	3.40	4.8	0.655	0.642		
	80 1	7.78	120	995	0.87	8	0.10	0	0.28	0.148	0.230	0.122	0.082	3.46	11.5	0.696	0.626		
	99.1	7.79	151	1000	0.87	8	0.10	0	0.34	0.133	0.208	0.110	0.074	3.11	6.5	0.580	0.558		
	85.1	7.78	120	1000	0.87	8	0.50	0	1.36	0.067	0.104	0.055	0.037	1.55	2.0	0.316	0.314	0.451	1.88
	82.1	7.88	450	1000	0.88	8	0.50	0	4.98	0.035	0.055	0.029	0.020	0.84	1.5	0.187	0.186		
	73.2	7.78	120	1005	0.41	8	0.50	0	1.36	0.067	0.115	0.061	0.041	1.75	14.0	0.434	-	0.461	1.97
	64.2	7.81	198	1015	0.43	8	0.50	0	2.24	0.052	0.091	0.048	0.032	1.36	2.0	0.234	0.232	0.516	1.33
	87.2	7.78	120	1000	0.41	8	0.50	0.05	1.36	0.067	0.115	0.061	0.041	1.75	0.5	0.264	0.264		
	67.2	7.80	179	1005	0.42	8	0.50	0.20	2.04	0.054	0.094	0.050	0.034	1.42	12.2	0.350	0.271	0.488	1.73
	104.1	9.94	600	1005	0.87	8	0.50	0	3.15	0.056	0.087	0.046	0.028	1.73	0.3	0.248	0.248		
↓	105.2	9.94	601	995	0.45	8	0.50	0	3.15	0.056	0.096	0.051	0.031	1.91	5.0	0.251	0.238	0.487	1.64
21-150	84.1	7.78	120	995	0.87	9	0.50	0	1.25	0.070	0.103	0.058	0.037	1.46	8.5	0.360	0.332	0.579	1.12
↓	86.2	7.78	121	1000	0.41	9	0.50	0	1.23	0.070	0.114	0.064	0.041	1.64	0.5	0.317	0.317		
	83.2	7.78	120	810	0.48	9	0.50	0	1.48	0.064	0.107	0.060	0.038	1.53	0.8	0.292	0.292		
	77.2	7.81	201	1020	0.43	9	0.50	0	1.98	0.055	0.091	0.051	0.033	1.29	0.4	0.249	0.249		
	62.2	7.81	200	1010	0.47	9	0.50	0	1.98	0.055	0.091	0.051	0.033	1.29	0.6	0.257	0.257		
↓	82.2	7.88	450	1000	0.47	9	0.50	0	4.37	0.038	0.061	0.034	0.022	0.88	0.7	0.191	0.191		
21-125	35	7.30	2000	600	0.88	15	1.50	0	72	0.009	0.010	0.007	0.004	0.09	0	0.183	0.183		
21-150	94.1	7.78	120	1000	0.87	15	0.10	0	0.15	0.203	0.228	0.167	0.086	2.30	4.5	0.685	0.676		
↓	75.1	7.88	448	1025	0.87	15	0.10	0	0.52	0.106	0.121	0.088	0.045	1.22	4.0	0.503	0.496		
	87.1	7.78	120	995	0.87	15	0.50	0	0.74	0.091	0.103	0.075	0.038	1.03	6.5	0.424	0.406	0.512	0.93
	76.2	7.81	200	1000	0.43	15	0.50	0	1.19	0.072	0.089	0.065	0.034	0.90	0.5	0.338	0.338		
↓	105.1	9.94	599	995	0.87	15	0.50	0	1.68	0.077	0.086	0.063	0.030	1.44	0.6	0.346	0.346		

b)

21-150	95.1	7.78	119	995	0.87	10	0.10	0	0.23	0.164	0.227	0.135	0.083	3.10	11.4	0.663	0.598		
↓	42	7.79	150	1010	0.87	10	0.10	0	0.28	0.148	0.205	0.122	0.075	2.82	5.5	0.669	0.654		
	64.1	7.81	199	1010	0.87	10	0.10	0	0.37	0.128	0.179	0.106	0.065	2.43	2.4	0.520	0.517		
	63.1	7.84	300	1015	0.87	10	0.10	0	0.54	0.106	0.148	0.088	0.053	2.02	5.0	0.456	0.443		
	47	7.94	799	999	0.88	10	0.10	0	1.40	0.067	0.093	0.055	0.034	1.30	4.0	0.307	0.299		
	70.1	7.78	121	1015	0.87	10	0.10	0.20	0.22	0.165	0.229	0.136	0.083	3.13	5.1	0.671	0.658		
↓	69.1	7.88	450	1000	0.87	10	0.10	0.20	0.83	0.087	0.120	0.071	0.043	1.66	2.0	0.366	0.364		
21-177	16	5.87	30	975	0.87	10	0.25	0	0.31	0.105	0.146	0.087	0.059	1.42	2.7	0.472	0.469		
↓	18	5.97	60	1000	0.88	10	0.25	0	0.57	0.078	0.110	0.065	0.044	1.09	1.2	0.374	0.373		
21-150	36	7.79	149	1015	0.87	10	0.25	0	0.68	0.094	0.131	0.078	0.048	1.80	9.5	0.438	0.393		
↓	38	7.84	299	1014	0.87	10	0.25	0	1.34	0.068	0.094	0.056	0.034	1.29	4.0	0.314	0.306		
21-177	17	5.87	30	950	0.87	10	0.50	0	0.62	0.074	0.103	0.061	0.042	1.01	2.0	0.371	0.369	0.470	1.27
21-144	26	5.96	55	1000	0.88	10	0.50	0	1.05	0.058	0.081	0.048	0.033	0.81	4.5	0.293	0.283		
↓	28	5.99	120	1010	0.88	10	0.50	0	2.21	0.040	0.056	0.033	0.023	0.56	6.0	0.248	0.230		
21-150	86.1	7.78	120	1000	0.87	10	0.50	0	1.11	0.074	0.103	0.061	0.037	1.41	1.5	0.336	0.335		
↓	49	7.79	150	1005	0.87	10	0.50	0	1.37	0.067	0.093	0.055	0.034	1.27	1.0	0.296	0.295		
21-150	57	7.80	180	1025	0.87	10	0.50	0.05	1.61	0.061	0.086	0.051	0.031	1.17	1.5	0.309	0.308	0.503	1.18
↓	55	7.80	180	1015	0.87	10	0.50	0	1.63	0.061	0.084	0.050	0.031	1.16	3.2	0.300	0.295	0.491	1.37
	56	7.80	180	1010	0.87	10	0.50	0	1.63	0.061	0.084	0.050	0.031	1.16	9.4	0.341	0.297	0.486	1.41
	67.1	7.80	180	1000	0.87	10	0.50	0	1.64	0.061	0.084	0.050	0.031	1.16	14.5	0.402	0.297	0.494	1.31
	68.1	7.80	181	1000	0.87	10	0.50	0	1.66	0.061	0.084	0.050	0.031	1.15	18.0	0.464	0.302	0.488	1.34
↓	72.1	7.80	182	1000	0.87	10	0.50	0	1.66	0.060	0.084	0.050	0.030	1.15	7.5	0.325	0.297	0.541	1.02
21-144	21	7.81	198	1000	0.87	10	0.50	0	1.80	0.058	0.081	0.048	0.029	1.11	9.0	0.315	0.275	0.628	0.52
↓	22	7.81	200	1000	0.87	10	0.50	0	1.82	0.058	0.081	0.048	0.029	1.10	5.0	0.283	0.271	0.619	0.49
	23	7.81	200	1010	0.87	10	0.50	0	1.82	0.058	0.081	0.048	0.029	1.10	8.8	0.310	0.271	0.499	1.27
	24	7.81	200	1000	0.87	10	0.50	0	1.82	0.058	0.081	0.048	0.029	1.10	6.0	0.295	0.277	0.690	0.10
21-150	100.1	7.78	204	485	0.87	10	0.50	0	3.69	0.041	0.062	0.037	0.022	0.85	0.4	0.214	0.214		
↓	32	7.84	298	1014	0.87	10	0.50	0	2.63	0.048	0.067	0.040	0.024	0.92	5.0	0.259	0.247	0.490	1.30
21-150	97.2	7.78	122	1065	0.41	10	0.50	0	1.05	0.076	0.116	0.069	0.042	1.59	1.0	0.317	0.316		
↓	98.2	7.78	121	1010	0.41	10	0.50	0	1.09	0.075	0.115	0.068	0.042	1.56	6.5	0.355	0.334	0.483	1.26
	33	7.84	300	1000	0.45	10	0.50	0	2.63	0.048	0.074	0.044	0.027	1.02	2.5	0.243	0.240	0.498	1.31
	74.2	7.94	799	1000	0.46	10	0.50	0	8.26	0.029	0.044	0.026	0.016	0.61	2.5	0.184	0.181	0.487	1.28
	101.2	9.83	401	1040	0.43	10	0.50	0	1.64	0.077	0.118	0.070	0.039	2.02	6.0	0.297	0.279	0.486	1.37
↓	103.2	9.94	601	1000	0.45	10	0.50	0	2.52	0.063	0.096	0.057	0.031	1.66	9.5	0.302	0.257	0.494	1.28
21-150	90.1	8.01	2005	1005	0.90	10	1.00	0	3.35	0.014	0.019	0.011	0.007	0.60	4.0	0.139	0.131	0.519	1.00
21-125	12	7.30	2000	600	0.90	10	1.50	0	109	0.007	0.010	0.006	0.004	0.12	0	0.110	0.110		
↓	11	7.30	2000	600	0.14	10	1.50	0	107	0.007	0.012	0.007	0.004	0.15	0	0.109	0.109		

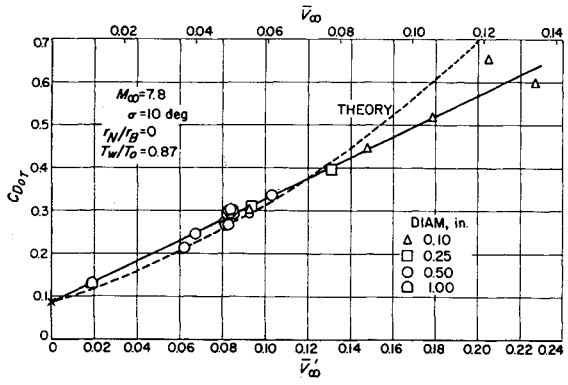

Fig. 10 Effect of viscous parameter on cone drag, base conditions.

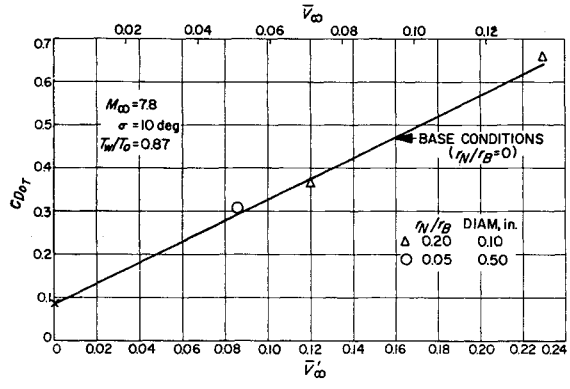

Fig. 11 Effect of nose bluntness on viscous cone drag.

used to reduce the data from the testing techniques employed. The scaling procedure is shown to be adequate by the duplicated drag at $\bar{V}_\infty' = 0.093$ for the 0.10-, 0.25-, 0.50-in. D cones.

The model construction method was to hollow out a cone from the base in order to obtain a desired volume of material and center-of-gravity location, thereby leaving an open chamber at the base. A model was used ($\bar{V}_\infty' = 0.093$) with this open chamber sealed off with a base plate. This base plate did not have any noticeable effect on the drag data.

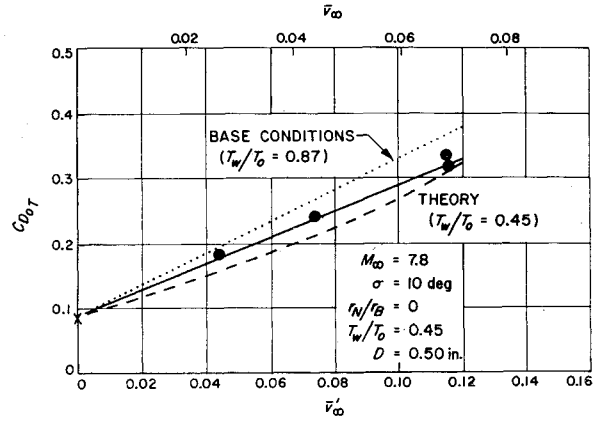

Fig. 12 Effect of wall temperature on viscous cone drag.

Also, models were launched with and without the holes, which were required for wire release. Again, this variation caused no perceptible effect on the data. The wire holes were the same diameter (0.015 in.) in the three sizes of models used to check the scaling parameter. Although the ratio of the hole size to model diameter varied by a factor of 5, the equivalent drag data indicate that the presence of the holes did not perturb the data.

Effects of various viscous parameters

For each parameter investigated, the drag appears to be a linear function of the viscous parameter $\bar{V}_\infty'$. These data are shown in Figs. 10–18. For convenience, a scale for the viscous parameter $\bar{V}_\infty$ is added to each figure. This allows for direct comparison of the data from this paper with the bulk of recently published data.[13,15] In all cases, the experimental data compare quite favorably with the included conical shock theoretical drag curves. The significant difference is that the experimental data lie on a straight line whereas the theoretical data form a parabolic-type curve. In all cases, the experimental linear fairings intersect the theoretical curves. A tabulation of these intercepts is shown in Table 3 along with a summary of the viscous drag slopes based upon a variety of hypersonic viscous parameters.

For the limited Mach range of the data in this paper there is not an obvious choice as to which intercept should be used as a constant in order to obtain meaningful theoretical drag

Table 3 Summary of viscous cone drag slopes from JPL data

σ (deg)	M_∞	T_w/T_0	$\beta_{\bar{V}_\infty'}$	$\beta_{\bar{V}_\infty}$	β	$\beta_{\bar{V}_c}$	$\beta_{\bar{X}_L}$	$\frac{d\left[C_{D_{O_T}}\right]}{d\left[M_\infty/(C_\infty R_{D_\infty})^{\frac{1}{2}}\right]}$	Number of Data Points	Intersection With Theory $\bar{V}'_\infty$	Intersection With Theory $\bar{X}_L$
10	5.9	0.87	2.48	4.18	3.46	6.10	0.253	1.70	5	0.116	1.19
6	7.8	0.45	2.06	4.49	4.11	5.91	0.128	1.73	5	0.112	1.90
6	7.8	0.87	2.52	5.49	4.54	7.23	0.157	1.73	3	0.107	1.82
8	7.8	0.45	1.86	3.51	3.21	5.23	0.125	1.56	2	0.093	1.48
8	7.8	0.87	2.43	4.58	3.79	6.82	0.163	1.66	6	0.116	1.84
9	7.8	0.45	2.02	3.59	3.28	5.60	0.141	1.69	5	0.113	1.72
9	7.8	0.87	2.52	4.48	3.71	6.99	0.176	1.73	1	0.115	1.75
10	7.8	0.45	1.98	3.34	3.06	5.55	0.146	1.66	4	0.125	1.77
10	7.8	0.87	2.40	4.04	3.35	6.71	0.177	1.65	21	0.118	1.67
15	7.8	0.45	1.96	2.68	2.45	5.24	0.198	1.64	1	0.117	1.22
15	7.8	0.87	2.35	3.21	2.66	6.27	0.237	1.61	3	0.118	1.23
8	9.9	0.45	1.91	3.61	3.31	6.00	0.098	1.60	1	0.100	2.03
8	9.9	0.87	2.24	4.23	3.51	7.03	0.114	1.54	1	0.082	1.66
10	9.9	0.45	1.79	3.02	2.76	5.48	0.104	1.50	2	0.093	1.64
15	9.9	0.87	2.25	3.08	2.55	6.45	0.187	1.54	1	0.087	1.05

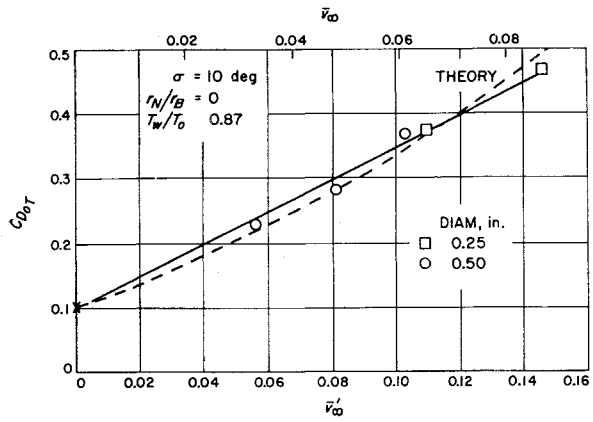

Fig. 13 Effect of Mach number on viscous cone drag (M = 5.9).

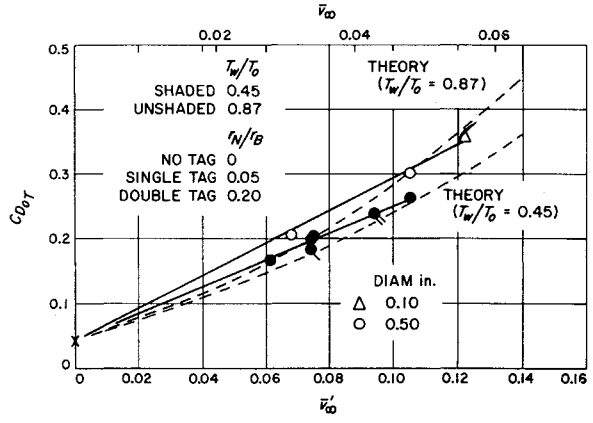

Fig. 15 Effect of cone angle on viscous drag (σ = 6°).

slopes. Therefore, nominal constant values of $\bar{V}_\infty' = 0.11$ and $\bar{\chi}_L = 1.6$ were each used in the summary plots of the JPL data. But when experimental data from other facilities extended into the higher Mach number regime ($M_\infty \approx 20$), the match with theory was much worse for $\bar{V}_\infty' = 0.11$ (where $\bar{\chi}_L \approx 3$) than for $\bar{\chi}_L = 1.6$. A similar divergence also occurs for both cone and wedge pressures; the experimental pressure data are essentially linear with $\bar{\chi}_L$ and are matched quite well by the weak interaction theory up to values of $\bar{\chi}_L$ of 2–3. For $\bar{\chi}_L > 3$, the theoretical pressures become progressively larger than the experimental.[4] The theory of Ref. 2 used for the viscous drag comparisons in this paper is for the weak interaction region and consequently is valid only for $\bar{\chi}_L = 0(1)$. Because of these considerations, the constant nominal value of $\bar{\chi}_L = 1.6$ rather than $\bar{V}_\infty' = 0.11$ is used for normalizing the experimental data in Table 4.

The effect upon drag of small nose bluntness (r_N/r_B = 0.05) is negligible for all values of the viscous parameter investigated. This result is the same as the effect of nose blunting at relatively high Reynolds numbers. At the low value of the viscous parameter (K = 0.007), data obtained at JPL by use of the free-flight wire-launch technique show minor effects on drag coefficient due to bluntness up to values of r_N/r_B = 0.13 for adiabatic-wall as well as the very cold-wall models (Fig. 19). The ratio of T_w/T_0 = 0.14 was obtained by cooling the aluminum models just prior to launch. This was done by spraying the models with liquid nitrogen while behind a wedge-shaped cooling shield (which requires about 0.1 sec to be retracted from the test-section flow) normally used for transient-type heat-transfer tests. In Fig. 19, the horizontal bars in the vicinity of the symbols at r_N/r_B = 0 are the conical shock theoretical drag values for the respective cold- and adiabatic-wall cases. The agreement between theory

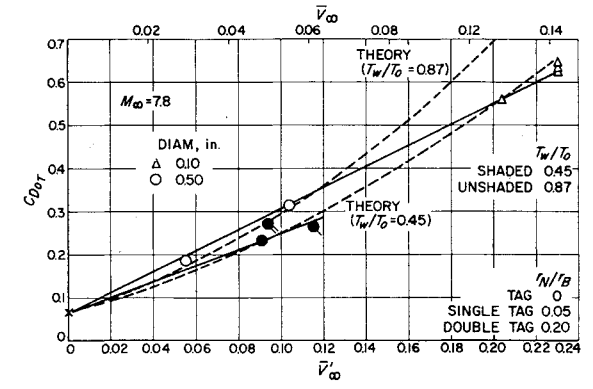

Fig. 16 Effect of cone angle on viscous drag (σ = 8°).

and experiment is quite good. The effect of the larger nose bluntness (r_N/r_B = 0.2) is insignificant for values of $\bar{V}_\infty' > 0.1$. When the longitudinal length is used in the definition of a viscous parameter for a blunted model, the length is that of a sharp-nose model with the same diameter.

A very orderly variation of the effects on drag for the parameters investigated (cone angle, wall-temperature ratio, Mach and Reynolds numbers) results from Figs. 10–18. The slopes of the linear drag coefficient curve for several viscous parameters as a function of cone angle are plotted in Fig. 20. Except for $\bar{V}_c$ (the cone-surface version of $\bar{V}_\infty$), the effect of cone angle is quite substantial when the viscous parameter is based upon the model length. When based upon the model base diameter, such as $\bar{V}_\infty'$, the cone angle effect becomes quite small.

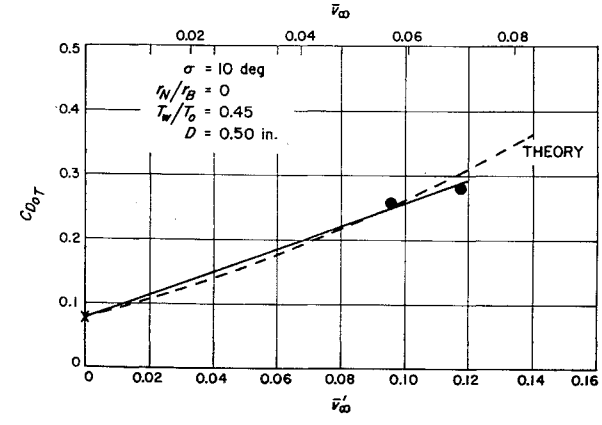

Fig. 14 Effect of Mach number on viscous cone drag (M = 9.9).

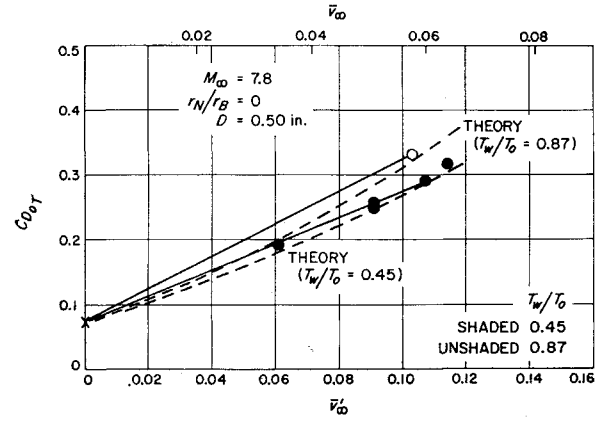

Fig. 17 Effect of cone angle on viscous drag (σ = 9°).

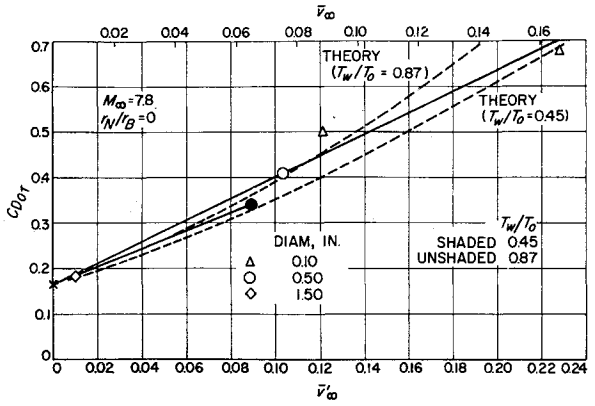

Fig. 18 Effect of cone angle on viscous drag (σ = 15°).

The effect of wall temperature on the drag slope is fairly insensitive to both cone angle and freestream Mach number. At $M_\infty = 7.8$, the ratios of the drag slopes of the cold-wall to the adiabatic-wall cones are shown in Fig. 21. Since the wall-temperature effect for the theoretical case is somewhat dependent upon the viscous parameter, the values of the viscous parameters are specified. The median value for the intercept of experimental with theoretical data is $\bar{V}_\infty' = 0.11$ (Table 3). The $\bar{\chi}_L = 1.6$ value is somewhat below the Table 3 mean in order to be more compatible with data at higher Mach numbers.[11,13,14]

The Mach number effect on the viscous drag slope is not defined adequately by the experimental data because of the scatter at $M_\infty = 9.9$. The comparison of the experimental results with conical shock theory ($\bar{V}_\infty' = 0.11$ and $\bar{\chi}_L = 1.6$) in Fig. 22 does not clear up the ambiguity. Theoretically, the Mach number effect is small when the viscous parameter $\bar{V}_\infty'$ is used (Fig. 7) and substantial (for $M_\infty < 10$) when $\bar{\chi}_L$ is used as the correlating viscous parameter. It is assumed that the $\bar{V}_\infty'$ theoretical curve is the best fit of the experimental data in Fig. 22.

Pitching Moment

The center-of-gravity location and the moment of inertia were experimentally measured for the 0.50-in. D models. The accuracy of the measurements were within $\pm 0.002L$ and $\pm 1\%$, respectively. When using the complete data reduction procedure, the accuracy of the oscillation frequency is within $\pm 1\%$. The data in Fig. 23 indicate a center-of-pressure location at about $0.705L$ from the nose of a sharp 10° cone and a normal force coefficient slope of 2.22/rad.

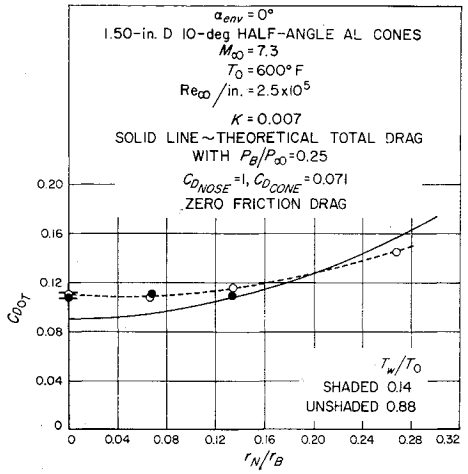

Fig. 19 Effect of cone nose bluntness on hypersonic free-flight cone drag.

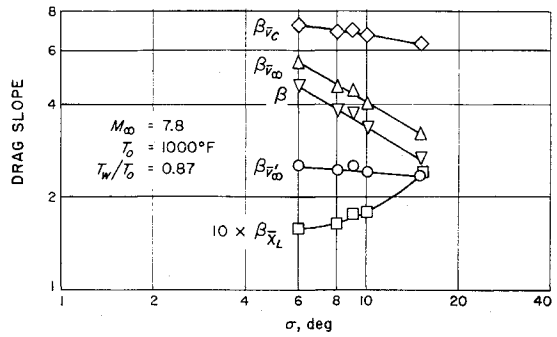

Fig. 20 Effect of cone angle on viscous drag slope.

The viscous normal force slope of 2.22/rad contrasts with the theoretical nonviscous case[24] of 1.875/rad, and the center-of-pressure appears to be about 2% of model length aft of the inviscid theoretical location ($0.667/\cos^2\sigma$) of $0.687L$. Data on the 8° half-angle cones of Ref. 14 also indicate, for the viscous case at small angles of oscillation ($\sigma_{env} < 5°$), a center-of-pressure location several percent aft of the theoretical location. These ballistic range data show that $C_{N\alpha}$/rad is larger than the theoretical value by about the same increment as for the data in Fig. 23.

Comparison of Cone Viscous Drag Data from Various Sources

Cone viscous drag measurements have been obtained for a wide range of parameters in several facilities using different techniques. The facilities represented are ballistic range,[12, 14] shock tunnel,[11] hotshot wind tunnel,[13] low-density hypervelocity tunnel,[13] and conventional hypersonic wind tunnel.[13,21] Except for the data of Refs. 12, 14, and 21 (where the model is in free-flight trajectory), the data are for sting-supported cones. Data from these facilities were plotted, and best-fit straight lines were used to determine the respective drag slopes as a function of some viscous parameter. This was done for uniform conditions of cone angle, model wall temperature and at very narrow ranges (±5%) of Mach number in order not to overlook possible effects of any of these parameters. Table 4 lists the drag slopes from the data of the forementioned references along with the data of this paper. All of the drag slopes have been normalized to $T_w/T_0 = \frac{1}{2}$ and to a 10° half-angle cone. The $\beta_{\bar{V}_\infty}'$ curve in Fig. 20 (which agrees quite well with theory) was used to normalize the data to σ = 10°. The normalization of wall-temperature ratio was based entirely on theory at $\bar{\chi}_L = 1.6$ for the specific conditions of each case. Each step of the normalization procedure is included in Table 4 in order that the relative effect of each step is indicated. The drag slope data are for cones having nose bluntness of $r_N/r_B = 0.03$ as

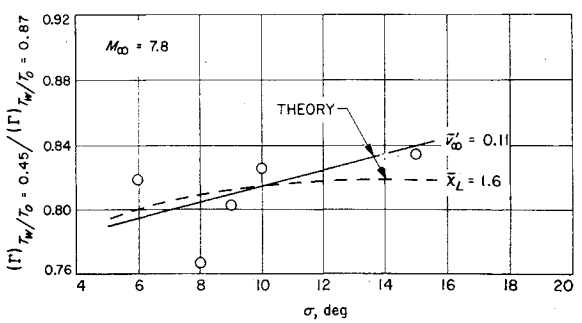

Fig. 21 Effect of wall temperature on viscous drag curve slope.

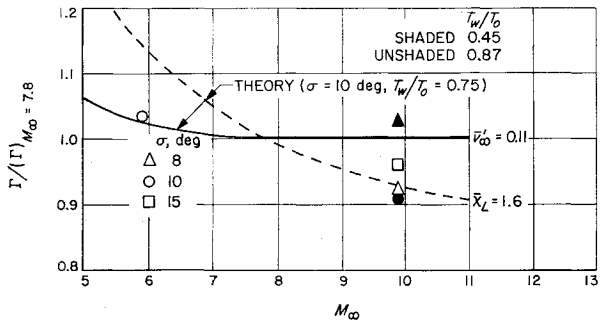

Fig. 22 Effect of Mach number on viscous drag curve slope.

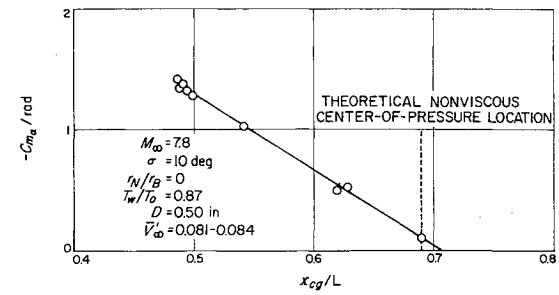

Fig. 23 Viscous cone static stability.

well as for sharp-nose cones. No identification of these nose bluntnesses is included as the JPL drag data, for the $r_N/r_B = 0.05$ cases are the same as for the sharp-nose cases.

The $\beta_{\bar{\nu}_\infty}$' data of Table 4 are presented in Fig. 24 along with a theoretical curve for $\bar{\chi}_L = 1.6$ (see Ref. 25 for another form of data comparison). It is noteworthy that the data of any one facility are self-consistent, i.e., grouped fairly well about some best-fit monotonic curve. But, the comparison of all of the data does create confusion as to the magnitude of Mach number effect and the level of the drag slopes. Of course, some of this discrepancy can be due to the normalizing process that, at best, is approximate. But, in the cases where data are obtained under similar conditions in different facilities, the normalization process does not contribute to the discrepancy. It is not clear as to what this confused comparison can be attributed: support (sting, free-flight), nozzle flow (uniform, nonuniform, divergent), model wall to total-temperature ratio, flow enthalpy (ballistic range, wind tunnel), manner of data acquisition, or the normalization procedure. In spite of the discrepancies, there does appear to be a definite effect of Mach number; the drag slopes decrease with increasing Mach number. This general trend is indicated by a shaded band in Fig. 24.

Summary

Hypersonic viscous effects on both total drag and static stability have been obtained for a large variety of parameters such as cone angle, nose bluntness, wall temperature, and Mach number. The free-flight test procedures used for acquiring these interference-free data have been described. The effect of the form of the correlating viscous parameter was investigated both experimentally and theoretically. The experimental drag data compare quite favorably with conical shock theory. Although a great deal of hypersonic viscous cone drag data have been obtained by various experimenters, the conditions are so varied that direct comparisons of the data are usually not practical. An attempt was made to compare all available data converted to a uniform condition by use of theoretically determined trends. In spite of the data scatter in this comparison, a very definite trend is

Table 4 Tabulation of viscous cone drag slopes from available data

Source	σ (deg)	M_∞	T_w/T_0	$\bar{\nu}'_\infty$ Range Min	Max	No. of Data Points	$\beta_{\bar{\nu}'_\infty}$	$\beta_{\bar{\nu}_\infty}$	$\beta_{\bar{\nu}'_\infty}$ Normalized to $T_w/T_0 = \frac{1}{2}$	$\beta_{\bar{\nu}'_\infty}$ Normalized to $T_w/T_0 = \frac{1}{2}$, σ = 10°	Symbol	Laboratory	Type of Facility	Nozzle	Model Support
Table 3	6	7.8	0.45	0.06	0.11	5	2.06	4.49	2.12	2.04	●	JPL	Hypersonic WT	Contoured	Free-Flight
	6	7.8	0.87	0.06	0.12	3	2.52	5.49	2.10	2.02	↓				
	8	7.8	0.45	0.09	0.12	2	1.86	3.51	1.92	1.89	▲				
	8	7.8	0.87	0.05	0.23	6	2.43	4.58	2.03	1.99					
	8	9.9	0.45	0.10		1	1.91	3.61	1.96	1.92					
	8	9.9	0.87	0.09		1	2.24	4.23	1.88	1.85	↓				
	9	7.8	0.45	0.06	0.12	5	2.02	3.59	2.07	2.05	■				
	9	7.8	0.87	0.10		1	2.52	4.48	2.11	2.09	↓				
	10	5.9	0.87	0.05	0.15	5	2.48	4.18	2.07	2.07	▼				
	10	7.8	0.45	0.04	0.12	4	1.98	3.34	2.03	2.03					
	10	7.8	0.87	0.02	0.23	21	2.40	4.04	2.01	2.01					
	10	9.9	0.45	0.09	0.12	2	1.79	3.02	1.84	1.84					
	15	7.8	0.45	0.09		1	1.96	2.68	2.01	2.07	◆				
	15	7.8	0.87	0.10	0.23	3	2.35	3.21	1.98	2.04					
	15	9.9	0.87	0.09		1	2.25	3.08	1.89	1.98	↓				
12	6.34	9.0	0.06	0.01	0.02	6	1.50	3.18	2.12	2.05	▨	NOL	Ballistic Range		Free-Flight
14	8	11.0	0.05	0.02		1	1.65	3.12	2.39	2.34	▨				
	8	11.7	0.04	0.01		2	1.63	3.08	2.38	2.34					
	8	12.5	0.04	0.02	0.04	3	1.15	2.18	1.68	1.65					
	8	13.0	0.04	0.02	0.10	7	1.27	2.40	1.86	1.83					
	8	15.1	0.03	0.10		3	1.07	2.02	1.61	1.58					
	8	16.2	0.03	0.10		2	0.95	1.80	1.43	1.40	↓				
11	6.5	13.7	0.1	0.20		1	0.94	2.07	1.24	1.21	⬡	CAL	Shock Tunnel	Contoured	Sting
	6.5	14.5	0.1	0.08	0.12	2	0.86	1.88	1.13	1.10	↓			Contoured	
	6.5	14.8	0.1	0.06		1	0.85	1.86	1.12	1.09	⬡			Conical	
	6.5	20.7	0.1	0.49		1	0.80	1.76	0.92	0.90					
	6.5	21.5	0.1	0.23	0.35	2	0.85	1.86	0.98	0.95					
	9	14.3	0.1	0.06	0.17	3	0.92	1.64	1.18	1.15	⬡				
13	6.34	14.7	0.1	0.07		1	0.97	2.05	1.27	1.23	☆	AEDC	Hot Shot Tunnel	Conical	Sting
	6.34	16.2	0.1	0.04		1	1.04	2.20	1.37	1.32	↓				
	6.34	17.3	0.1	0.05	0.08	3	0.92	1.95	1.21	1.17					
	9	16.1	0.1	0.05		1	1.13	2.02	1.50	1.49	⬡				
	9	17.0	0.1	0.10	0.13	3	1.07	1.90	1.42	1.41					
	9	17.3	0.1	0.06	0.08	3	1.04	1.85	1.38	1.37					
	9	18.0	0.1	0.13		1	0.93	1.65	1.24	1.23					
	9	21.7	0.1	0.05	0.24	11	1.07	1.90	1.42	1.41	↓				
	9	10.1	0.75	0.02	0.08	11	1.76	3.12	1.56	1.54	⬡		Hypersonic WT	Contoured	
	9	9.0	0.20	0.40	0.46	5	1.35	2.41	1.65	1.62	⬡		Hypervelocity LD	Conical	
	9	9.4	0.25	0.30	0.35	6	1.37	2.45	1.60	1.59	↓		Hypervelocity LD	Conical	
15	10	10.0	0.33	0.06	0.09	7	1.48	2.50	1.63	1.63	☆		Hypersonic WT	Contoured	Free-Flight

WT - Wind Tunnel
LD - Low Density WT

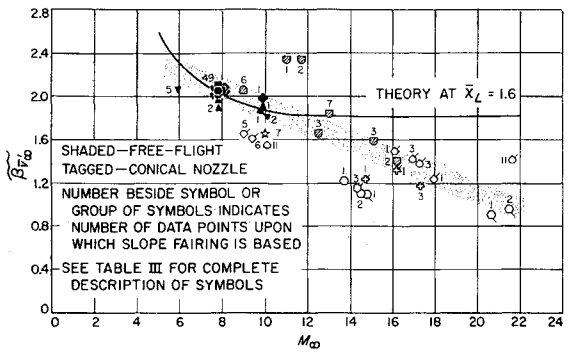

Fig. 24 Effect of M_∞ on $\tilde{\beta}_{\bar{V}_\infty}$' (summary of available viscous drag data).

established: the viscous drag slope decreases with increasing Mach number.

References

[1] Lees, L. and Probstein, R. F., "Hypersonic viscous flow over a flat plate," Rept. 195, Aero Engineering Lab., Princeton Univ. (April 1952).

[2] Probstein, R. F., "Interacting hypersonic laminar boundary layer flow over a cone," TR AF 279811, Div. of Engineering, Brown Univ., Armed Services Technical Information Agency AD 66 227 (March 1955).

[3] Probstein, R. F. and Elliott, D., "Transverse curvature effect in compressible axially symmetric laminar boundary-layer flow," J. Aeronaut. Sci. **23**, 208–224 (1956).

[4] Hayes, W. D. and Probstein, R. F., *Hypersonic Flow Theory* (Academic Press Inc., New York, 1959).

[5] Cheng, H. K., "Hypersonic flow with combined leading-edge bluntness and boundary-layer displacement effect," Cornell Aeronautical Lab. Rept. AF-1285-A-4, Armed Services Technical Information Agency AD 243140 (August 1960).

[6] Yaushara, M., "Axisymmetric viscous flow past very slender bodies of revolution," J. Aerospace Sci. **29**, 667–679 (1962).

[7] Dewey, C. F., Jr., "Bluntness and viscous-interaction effects on slender bodies at hypersonic speeds," Rand Corp. Memo. RM-3832-PR (September 1964).

[8] Langelo, V. A. and Lengyel, A., "Aerodynamic coefficients of a pointed cone at angles of attack in rarefied gas flow," General Electric Co. Technical Information Series, GE R58SD229 (May 1958).

[9] "Experimental investigation of the aerodynamic characteristics of 9° half-angle cones with varying degrees of nose bluntness at Mach number 9," Aeronutronic, A Division of Ford Motor Co., Publ. U-1638 (April 1962).

[10] Bloxsom, D. E. and Rhodes, B. V., "Experimental effect of bluntness and gas rarefaction on drag coefficients and stagnation heat transfer on axisymmetric shapes in hypersonic flow," J. Aerospace Sci. **29**, 1429–1432 (1962).

[11] Wilkinson, D. B. and Harrington, S. A., "Hypersonic force, pressure, and heat transfer investigations of sharp and blunt slender cones," Arnold Engineering Development Center AEDC-TDR 63-177 (August 1963).

[12] Crogan, L. E., "Drag and stability data obtained from free-flight hypersonic firings of both pointed and blunt nosed 12°40′ total angle cones at several range pressures," Naval Ordnance Lab. TR 63-36 (1963).

[13] Whitfield, J. D. and Griffith, B. J., "Viscous effects on zero-lift drag of slender blunt cones," Arnold Engineering Development Center AEDC-TDR-63-35 (March 1963); also "Hypersonic viscous drag on blunt slender cones," AIAA J. **2**, 1714–1722 (1964).

[14] Lyons, W. C., Jr., Brady, J. J., and Levensteins, Z. J., "Hypersonic drag, stability, and wake data for cones and spheres," AIAA J. **2**, 1948–1956 (1964).

[15] Griffith, B. J. and Siler, L. G., "Comparisons of free-flight and wind tunnel data on slender cones," Arnold Engineering Development Center AEDC-TDR-64-272 (December 1964).

[16] Dayman, B., Jr., "Simplified free-flight testing in a conventional wind tunnel," Jet Propulsion Lab. TR 32-246 (October 1962).

[17] Dayman, B., Jr., "Optical free-flight wake studies," Jet Propulsion Lab. TR 32-364 (November 1962).

[18] Ashkenas, H., private communication, Fluid Physics Sec. Jet Propulsion Lab. (August 1963).

[19] Seiff, A., "A new method for computing drag coefficients from ballistic range data," J. Aeronaut. Sci. **25**, 133–134 (1958).

[20] Jaffe, P., "Obtaining free-flight dynamic damping of an axially symmetric body (at all angles-of-attack) in a conventional wind tunnel," Jet Propulsion Lab., TR 32-544 (January 1964).

[21] Dayman, B., Jr., "Free-flight hypersonic viscous effects on slender cones," AIAA Preprint 64-46 (January 1964).

[22] "Wind tunnel facilities," Jet Propulsion Lab., Wind Tunnel Staff, Tech. Release 34–257 (April 18, 1961).

[23] Mack, L. M., "Direct numerical solution of flat plate laminar boundary layer equations," Jet Propulsion Lab., private communiqué (April 1963).

[24] Kopal, Z., "Tables of supersonic flow around cones," Dept. of Electrical Engineering, Center of Analysis, Massachusetts Institute of Technology, TR 1 (1947).

[25] White, C. O., "Zero angle of attack drag of cones in hypersonic low density flow," Aeronutronic Rept. U-1794 (August 1962).